**SUPPORTING INFORMATION**

**for**

# Kinetic Analysis of the Conversion of Nonheme Alkylperoxoiron(III) Species to Iron(IV) Complexes

Michael P. Jensen, Antoni Mairata i Payeras, Adam T. Fiedler, Miquel Costas, József Kaizer, Audria Stubna, Eckard Münck,* and Lawrence Que, Jr.*

Contribution from the Department of Chemistry and the Center for Metals in Biocatalysis, University of Minnesota, Minneapolis, Minnesota 55455 and the Department of Chemistry, Carnegie Mellon University, Pittsburgh, Pennsylvania 15213

**Table S1**. Temperature-dependent kinetic data.

| **5Me$_3$TPA in acetone** | | | | |
|---|---|---|---|---|
| **T ($^o$C)** | **[Fe$^{II}$]$_0$ (mM)** | **[$^t$BuOOH]$_0$ (equiv/Fe)** | **$10^3$ $k_{fast,obs}$ ($s^{-1}$)** | **$10^3$ $k_{slow,obs}$ ($s^{-1}$)** |
| -35 | 0.92 | 10 | (fast) | 12(1) |
| -40 | 0.87 | 10 | (fast) | 5.8(3) |
| -45 | 1.1 | 10 | 118(2) | 2.86(6) |
| -50 | 1.0 | 10 | 58.0(6) | 1.47(2) |
| -55 | 1.2 | 10 | 34.1(4) | 0.93(2) |
| -60 | 0.96 | 10 | 9.6(1) | 0.40(1) |
| **TPA in acetone** | | | | |
| -30 | 1.6 | 10 | (fast) | 12.0(1) |
| -40 | 1.8 | 10 | 121(6) | 3.76(4) |
| -40 | 1.2 | 10 | 45.4(3) | 2.9(3) |
| -40 | 2.2 | 10 | 65.6(5) | 3.27(9) |
| -50 | 2.1 | 10 | 31.7(2) | 0.95(1) |
| -50 | 2.0 | 10 | 22.4(1) | 0.91(3) |
| -50 | 1.0 | 20 | 23.0(1) | 1.24(4) |
| -50 | 0.5 | 40 | 25.1(2) | 1.1(4) |
| -60 | 1.6 | 10 | 5.3(1) | 0.22(3) |
| **BPMCN in $CH_3CN$** | | | | |
| -26 | 0.85 | 2 | 84(2) | 7.7(2) |
| -32 | 0.58 | 2 | 52.7(6) | 4.9(2) |
| -36 | 0.58 | 2 | 35.6(3) | 2.26(9) |
| -36 | 0.85 | 2 | 32.9(3) | 2.00(7) |
| -40 | 0.58 | 2 | 20.2(2) | 1.61(6) |
| -42 | 0.85 | 2 | 20.3(2) | 1.66(6) |
| -45 | 0.61 | 2 | 7.88(8) | 0.92(1) |
| **BPMCN in $CH_2Cl_2$** | | | | |
| -55 | 0.58 | 10 | 14.5(8) | 2.48(3) |
| -60 | 0.58 | 10 | 5.2(3) | 1.37(3) |
| -65 | 0.58 | 10 | 2.45(4) | 0.633(6) |
| -67 | 0.71 | 5 | 1.20(5) | 0.367(9) |
| -67 | 1.3 | 5 | 1.7(1) | 0.301(6) |

| **BPMCN in $CH_2Cl_2$ (continued)** | | | | |
|---|---|---|---|---|
| -67 | 1.8 | 5 | 1.73(6) | 0.522(7) |
| -67 | 3.3 | 5 | 1.67(8) | 0.62(2) |
| -70 | 0.58 | 10 | 0.98(1) | 0.387(2) |
| -75 | 0.58 | 10 | 0.376(3) | 0.214(1) |

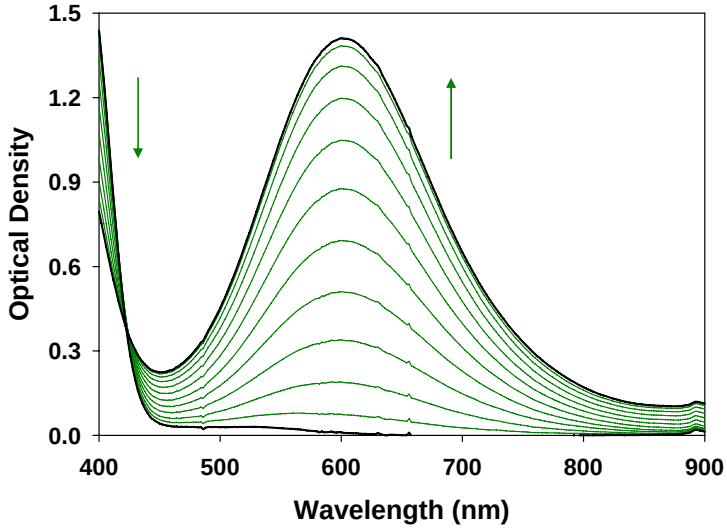


**Figure S1**. Time-dependent vis-NIR absorption data for oxidation of $Fe^{II}$(β-BPMCN)$(OTf)_2$ (0.61 mM) with $^{t}$BuOOH (1.2 mM) in the presence of $H_2O$ (0.3 M) to an alkylperoxoiron(III) intermediate in $CH_3CN$ at 228 K.

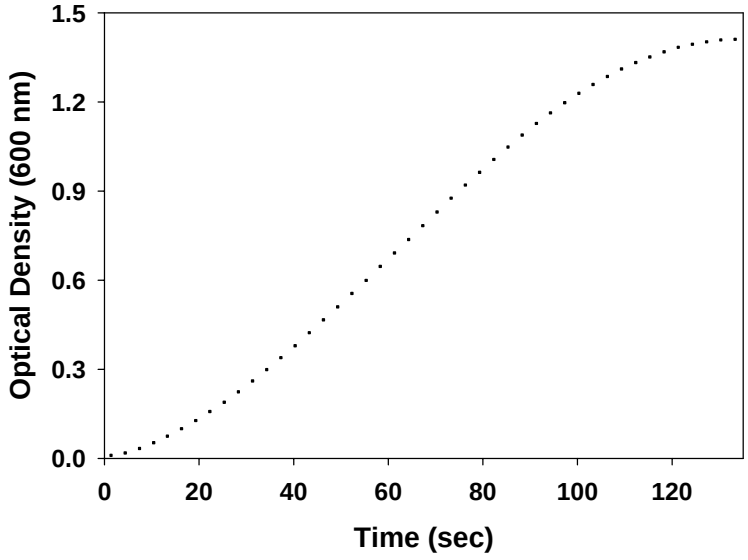


**Figure S2**. Time dependent optical density at 600 nm for data shown in Figure S1 above.

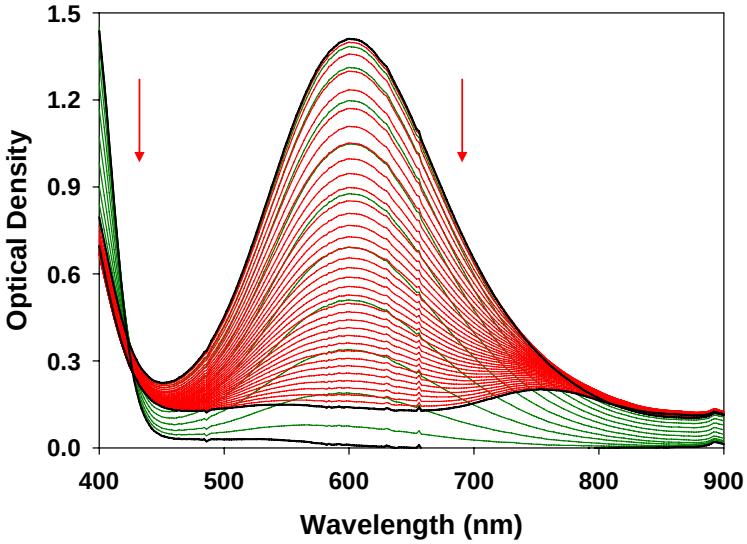


**Figure S3**. Time-dependent vis-NIR data for decay of the alkylperoxoiron(III) intermediate supported by β-BPMCN (red, Figure 7A) superimposed on its prior accumulation (green, Figure S1).

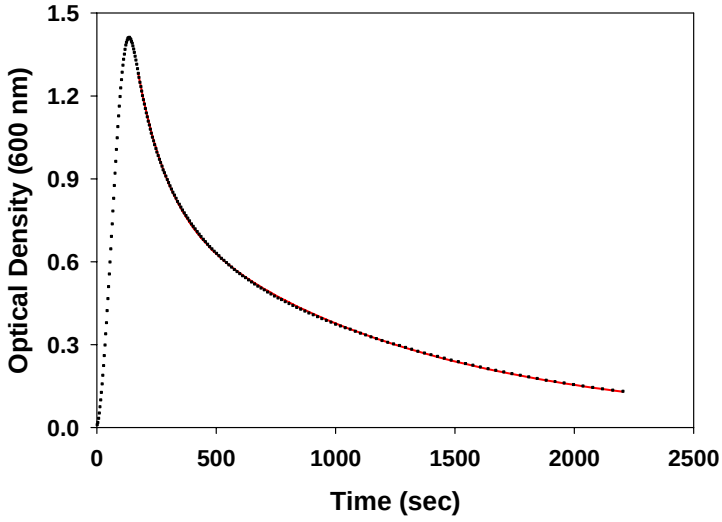


**Figure S4**. Time dependent optical density at 600 nm for data shown in Figure S3 above. Red curve is the calculated kinetic fit for decay of alkylperoxoiron(III) to oxoiron(IV) (Figure 8).

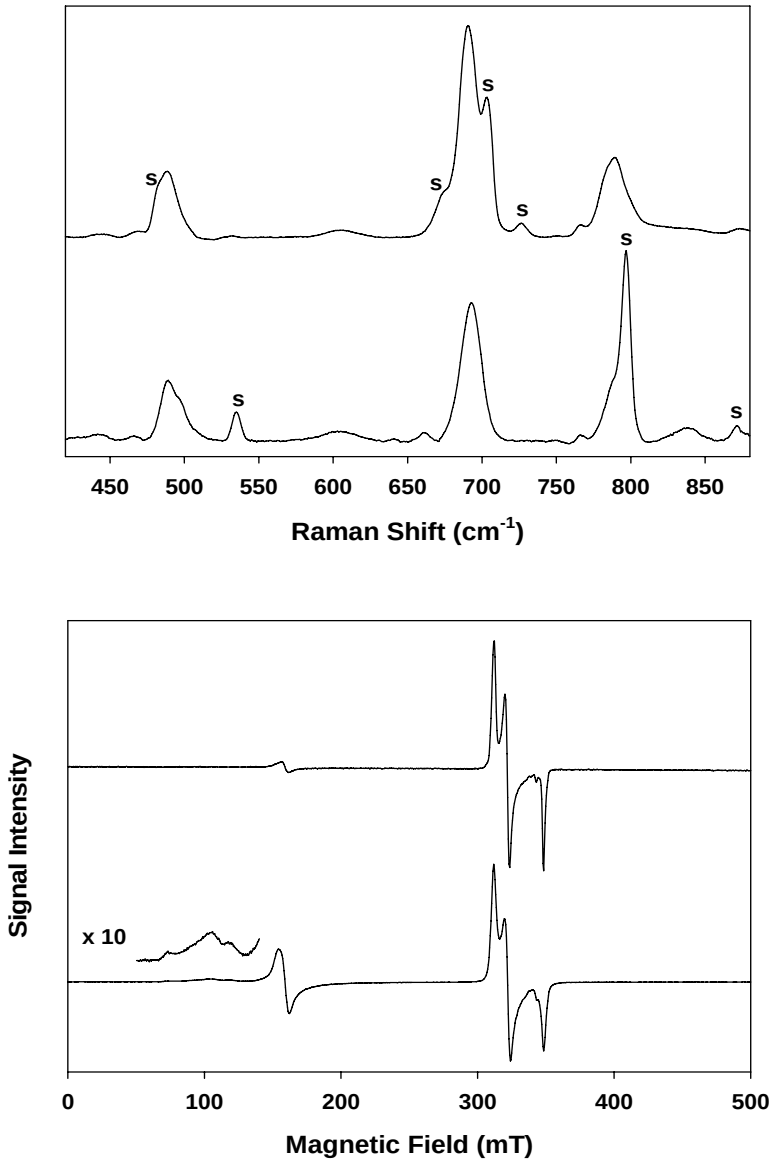


**Figure S5**. Resonance Raman (top panel, 568.2 nm laser excitation, solvent features are denoted ('s')) and EPR spectra (bottom) of alkylperoxoiron(III) intermediates supported by 5-$Me_3$TPA (top spectra in each panel) and TPA (bottom) in frozen acetone ($d^6$-acetone for the Raman spectrum of the 5-$Me_3$TPA intermediate) at 77 and 4.0 K, respectively.

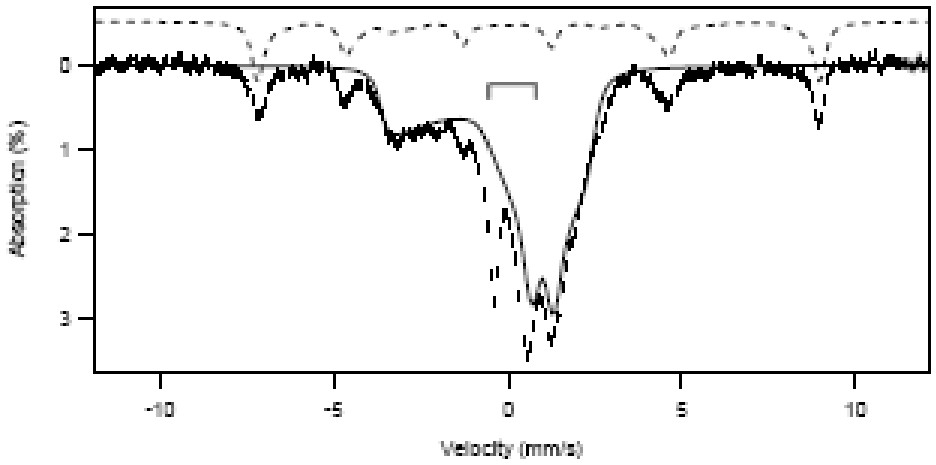


**Figure S6**. Mössbauer spectrum of an aliquot taken from the oxidation reaction of $Fe^{II}$(5-$Me_3$TPA)$(OTf)_2$ (1.67 mM) with 10 equiv. $^t$BuOOH in acetone, freeze-quenched at the timepoint corresponding to maximum extinction of the alkylperoxoiron(III) LMCT chromophore.

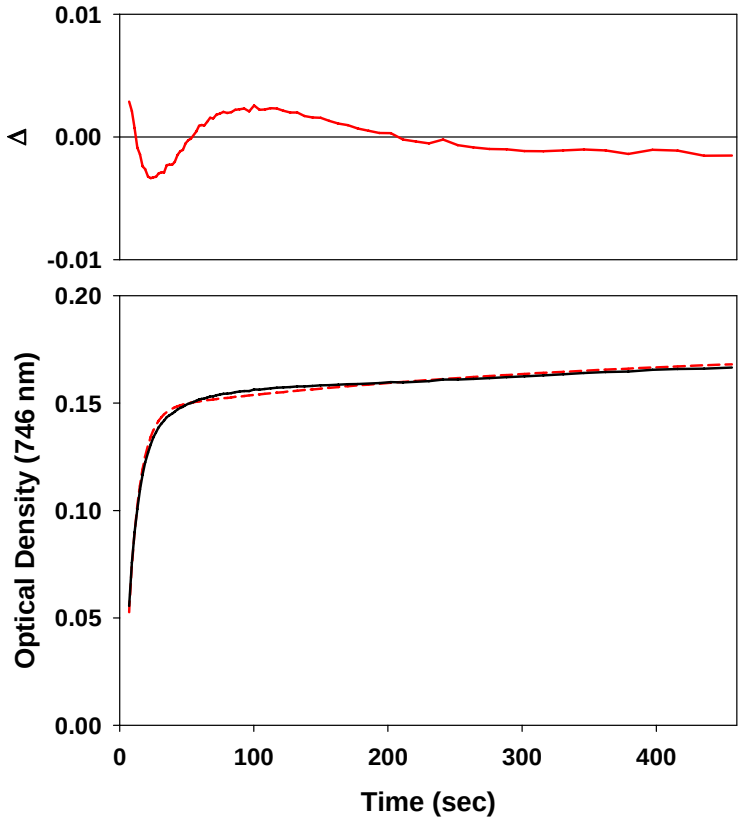


**Figure S7**. Observed (black) vs. calculated (red) optical density at 746 nm for conversion of the alkylperoxoiron(III) intermediate supported by 5-$Me_3$TPA to oxoiron(IV) in acetone at 228 K, data shown in Figure 1.

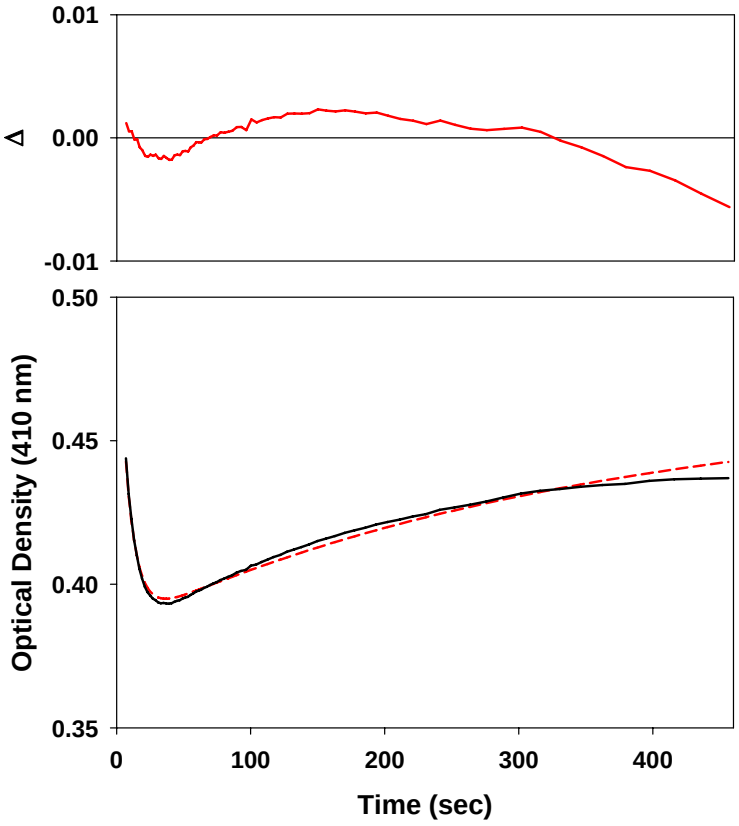


**Figure S8**. Observed (black) vs. calculated (red) optical density at 410 nm for conversion of the alkylperoxoiron(III) intermediate supported by 5-$Me_3$TPA to oxoiron(IV) in acetone at 228 K, data shown in Figure 1.

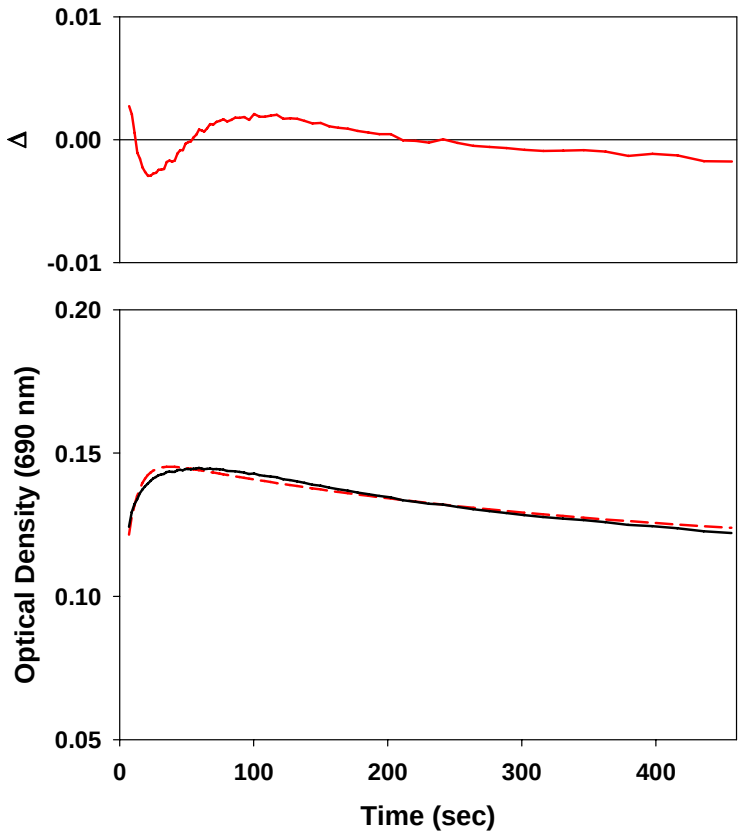


**Figure S9**. Observed (black) vs. calculated (red) optical density at 690 nm for conversion of the alkylperoxoiron(III) intermediate supported by 5-$Me_3$TPA to oxoiron(IV) in acetone at 228 K, data shown in Figure 1.

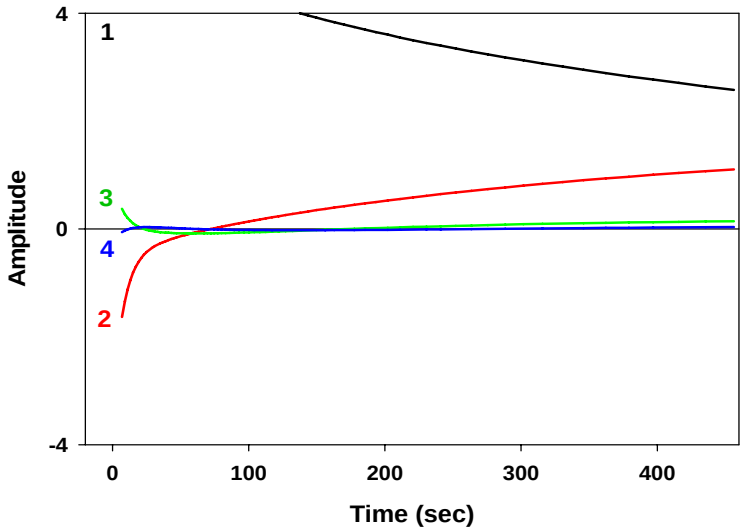


**Figure S10**. Weighted kinetic vectors (**U x S**) from SVD of dataset in Figure 1 for conversion of the alkylperoxoiron(III) intermediate supported by $Me_3TPA$ to oxoiron(IV) in acetone at 228 K. For technical explanation of SVD and the global fitting, see reference 50.

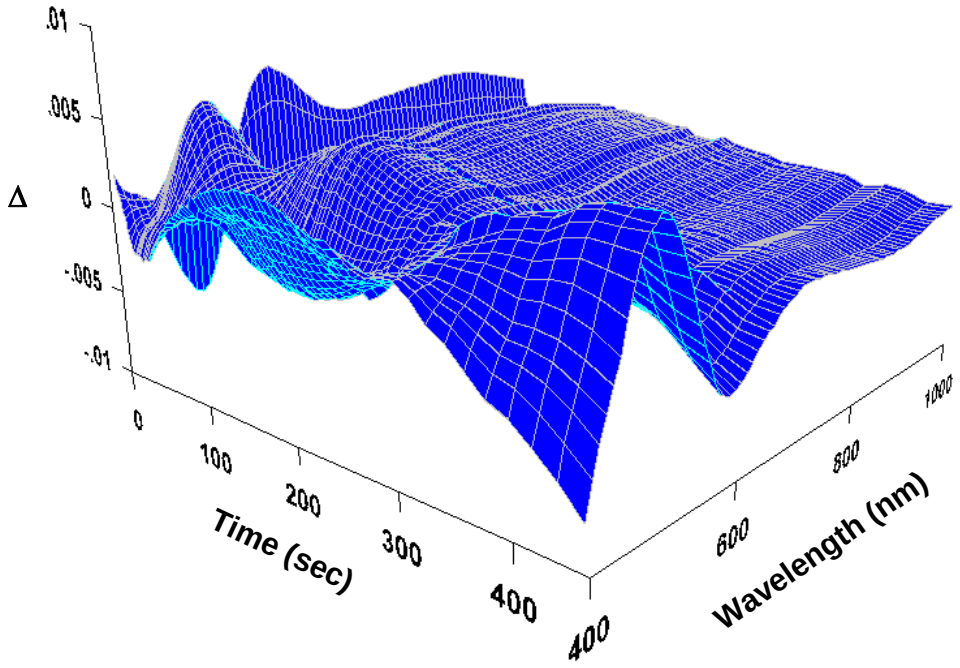


**Figure S11**. Global residuals from kinetic fit of dataset in Figure 1 (5-$Me_3TPA$/acetone).

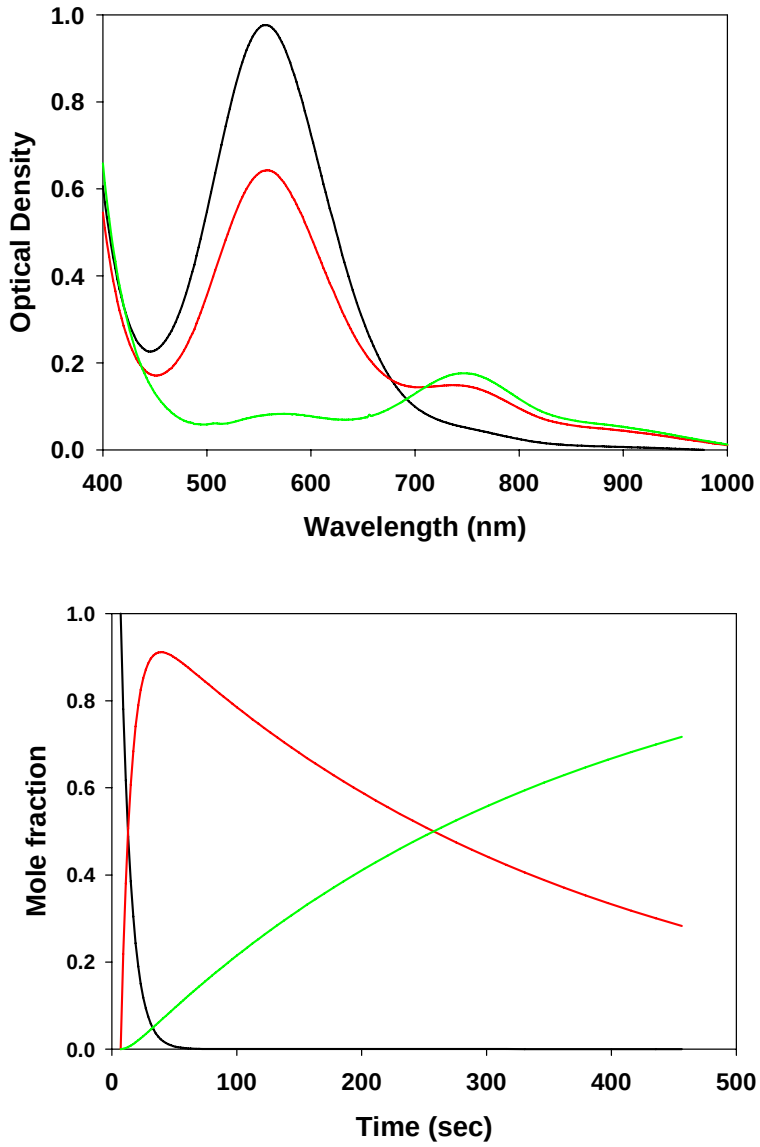


**Figure S12**. Calculated spectra (top) and time-dependent concentrations (bottom) for a sequential A → B → C kinetic model to the time dependent optical data for conversion of the alkylperoxoiron(III) intermediate supported by 5-$Me_3$TPA to oxoiron(IV) shown in Figure 1.

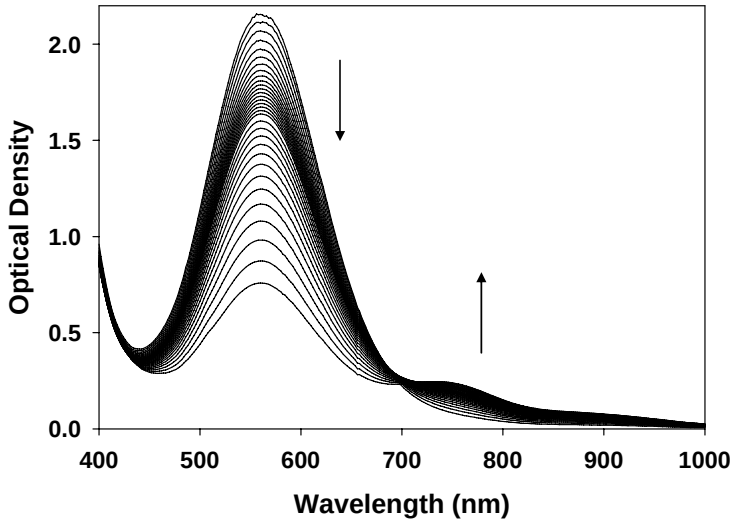


**Figure S13**. Time dependent visible-NIR spectra for conversion of the alkylperoxoiron(III) intermediate supported by TPA to oxoiron(IV) in acetone at 223 K.

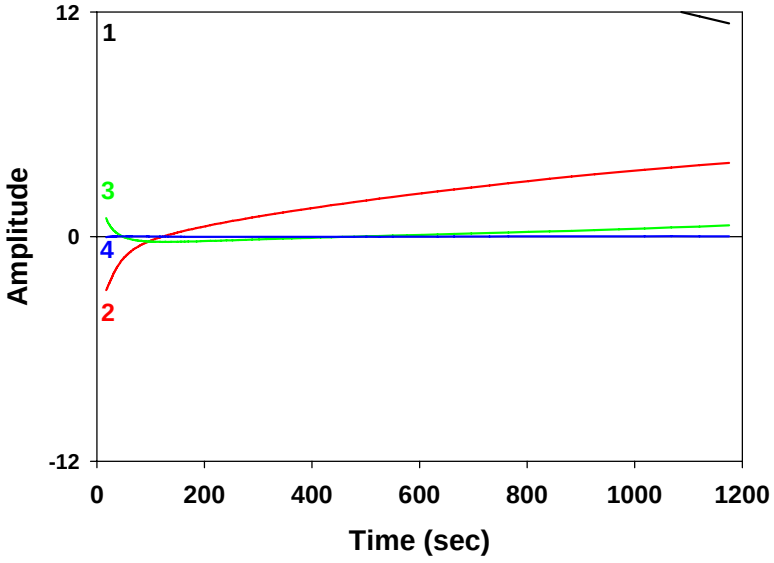


**Figure S14**. Weighted kinetic vectors (**U x S**) from SVD of dataset in Figure S13 for conversion of the alkylperoxoiron(III) intermediate supported by TPA to oxoiron(IV) in acetone at 223 K.

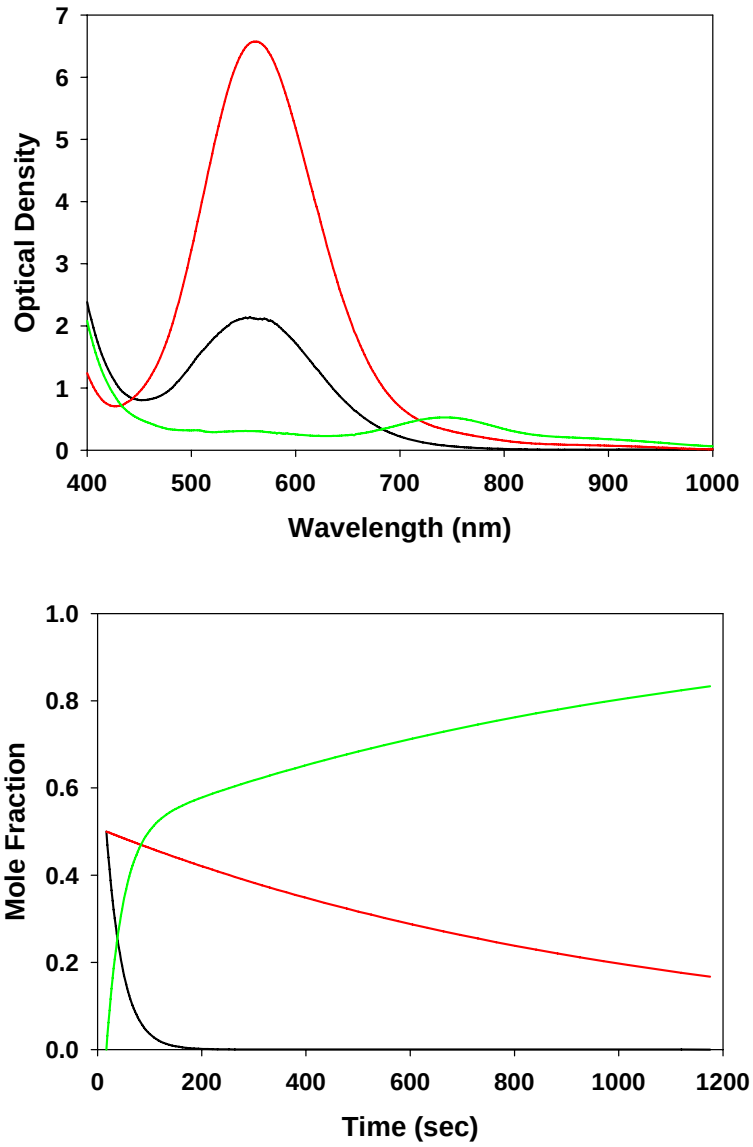


**Figure S15**. Calculated spectra (top) and time-dependent concentrations (bottom) for a sequential A → C, B → C kinetic model to the time-dependent optical data shown in Figure S13 for decomposition of the alkylperoxoiron(III) intermediate supported by TPA to oxoiron(IV) in acetone at 223 K, with mole fractions arbitrarily set to $[A]_0 = 0.50$, $[B]_0 = 0.50$, $[C]_0 = 0$.

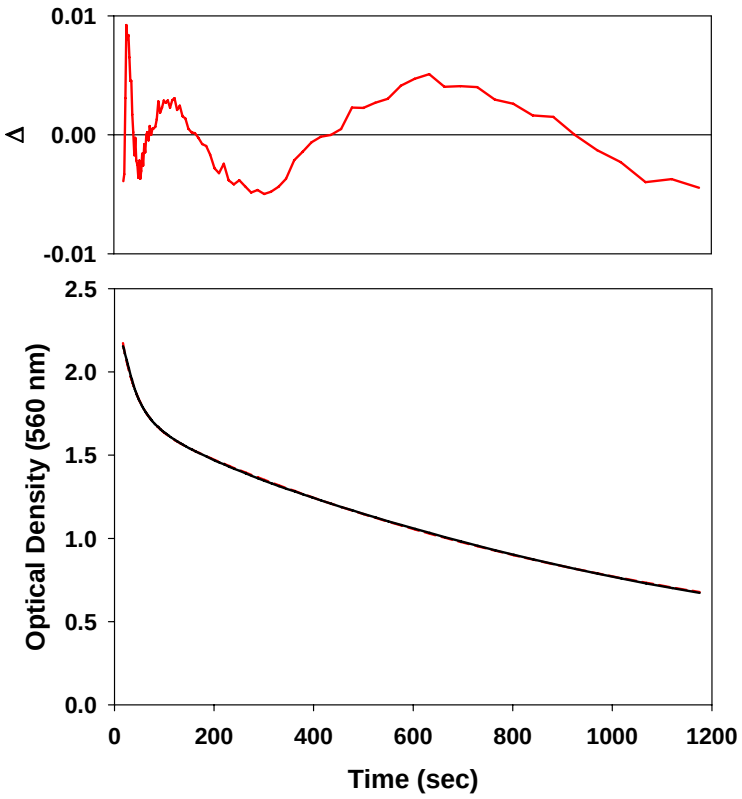


**Figure S16**. Observed (black) vs. calculated (red) optical density at 560 nm for conversion of the alkylperoxoiron(III) intermediate supported by TPA to oxoiron(IV) in acetone at 223 K, data shown in Figure S13.

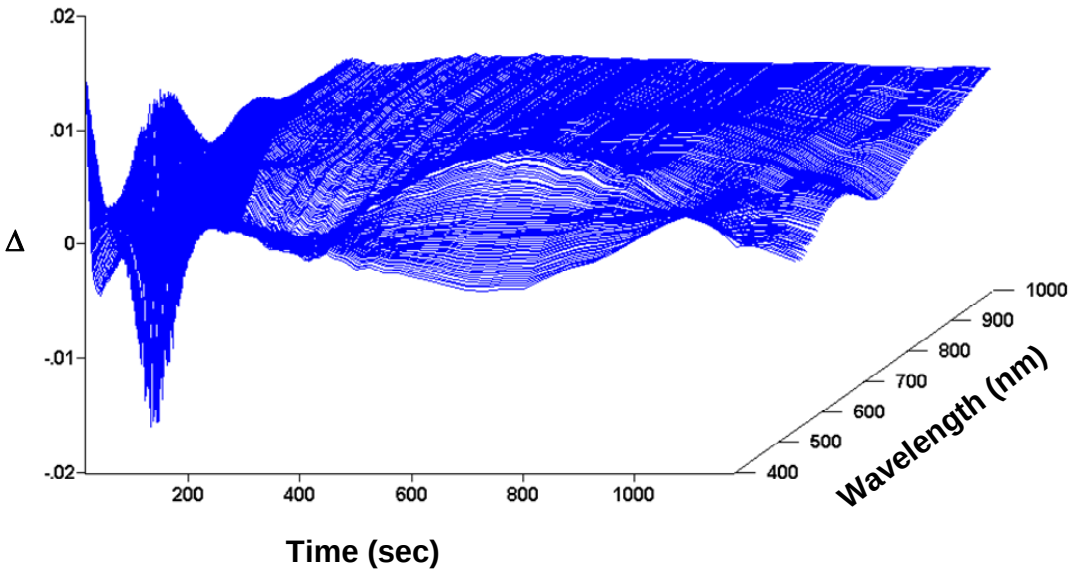


**Figure S17**. Global residuals from kinetic fit of dataset in Figure S13 (TPA/acetone).

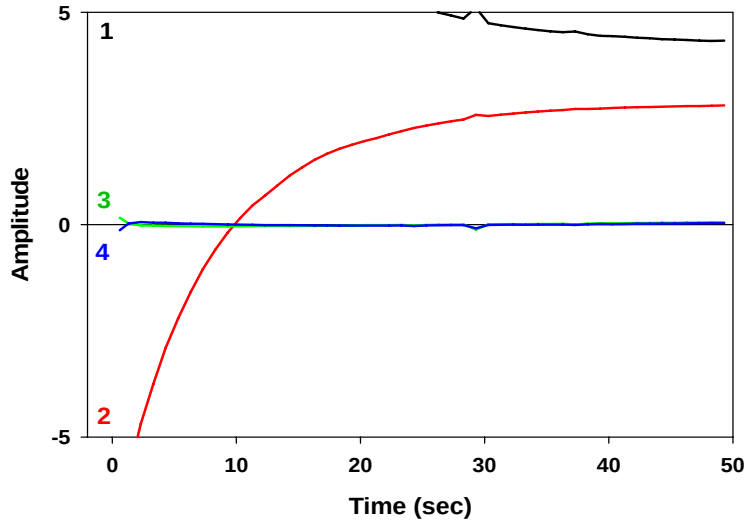


**Figure S18**. Weighted kinetic vectors (**U x S**) from SVD of dataset in Figure 4 for conversion of the alkylperoxoiron(III) intermediate supported by TPA to oxoiron(IV) in $CH_3CN$ with added pyridine-*N*-oxide at 228 K.

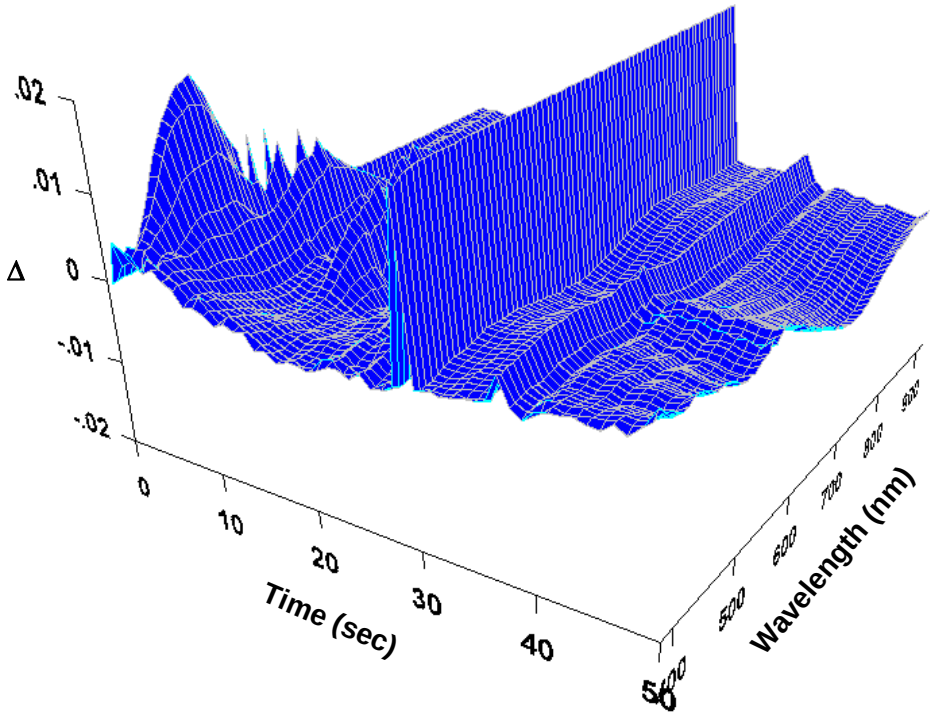


**Figure S19**. Global residuals from kinetic fit of dataset in Figure 4 (TPA/pyridine-N-oxide/$CH_3CN$).

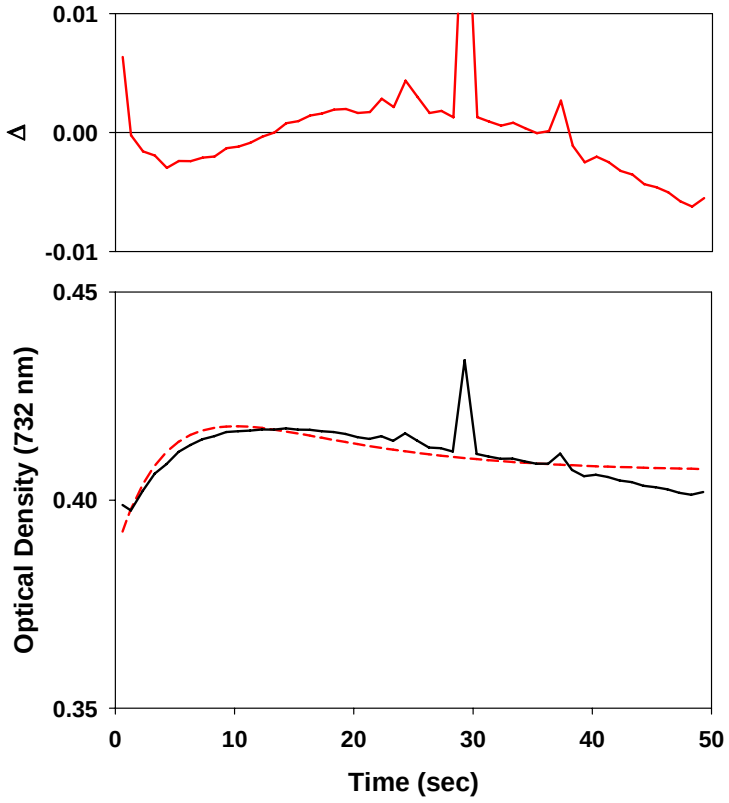


**Figure S20**. Observed (black) vs. calculated (red) optical density at 732 nm for conversion of the alkylperoxoiron(III) intermediate supported by TPA to oxoiron(IV) in $CH_3CN$ with added pyridine-*N*-oxide at 231 K shown in Figure 4K For comparison see Figure S9.

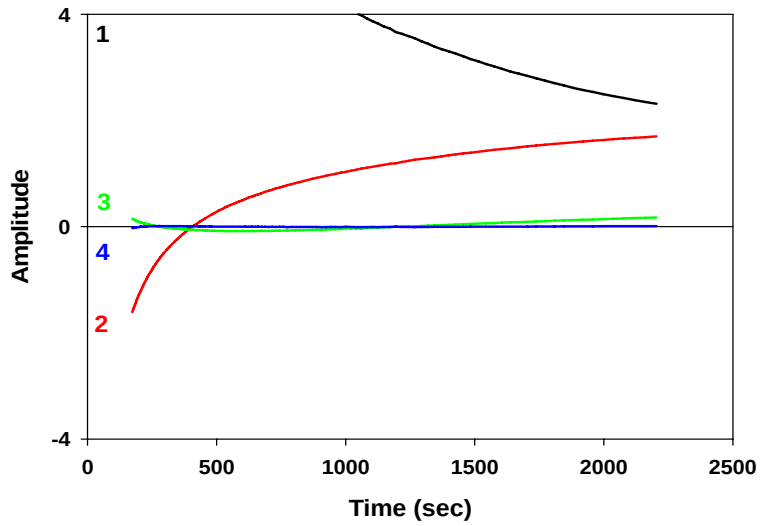


**Figure S21**. Weighted kinetic vectors (**U x S**) from SVD of dataset in Figure 7A for conversion of the alkylperoxoiron(III) intermediate supported by β-BPMCN to oxoiron(IV) in $CH_3CN$ with added $H_2O$ at 223 K.

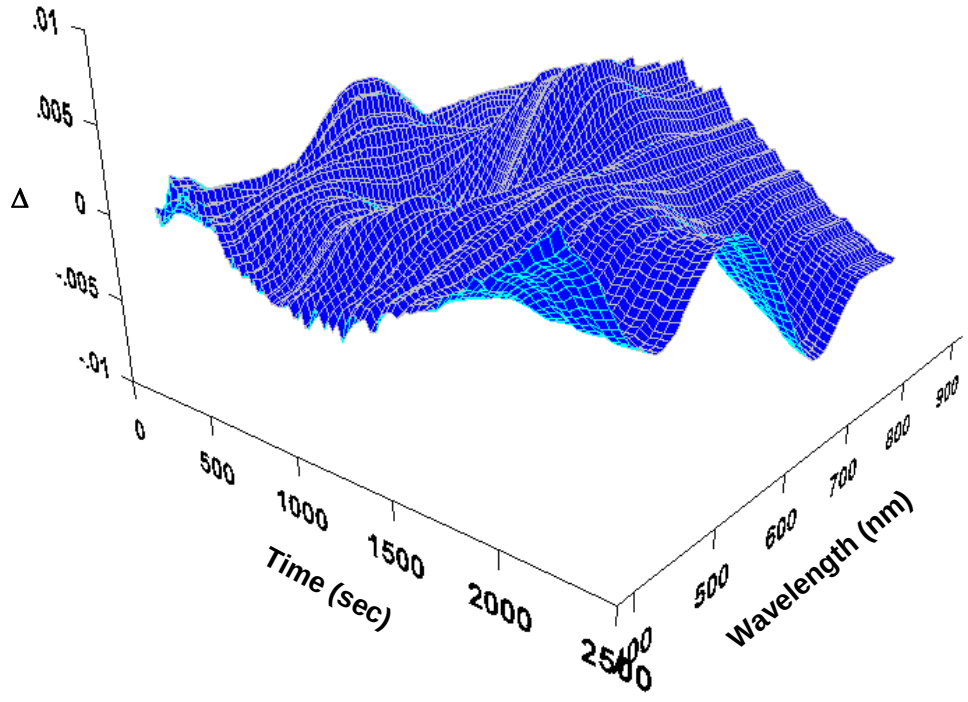


**Figure S22**. Global residuals from kinetic fit of dataset in Figure 7A (β-BPMCN/$H_2O$/$CH_3CN$).

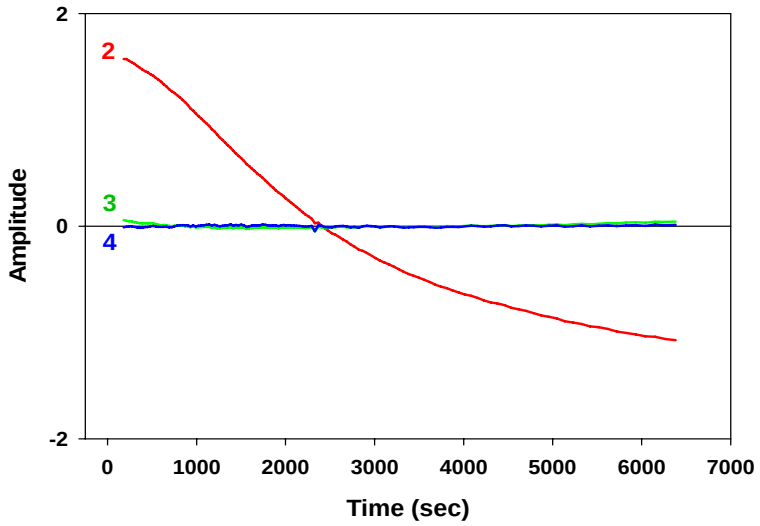


**Figure S23**. Weighted kinetic vectors (**U x S**) from SVD of dataset in Figure 7B for conversion of the alkylperoxoiron(III) intermediate supported by β-BPMCN to alkylperoxoiron(IV) in $CH_2Cl_2$ at 228 K.

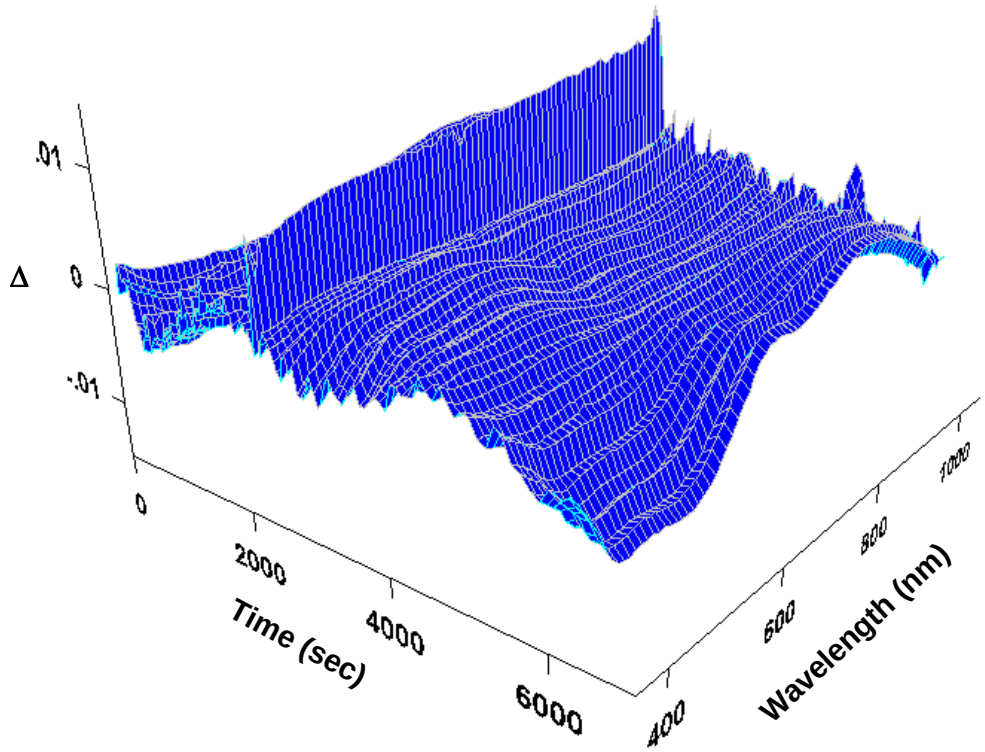


**Figure S24**. Global residuals from kinetic fit of dataset in Figure 7B (β-BPMCN/$CH_2Cl_2$).